

Plasma effects in a micromachined floating-gate high-electron-mobility transistor

Y. Hu and I. Hagiwara

*Department of Mechanical Sciences and Engineering,
Tokyo Institute of Technology, Tokyo 152-8552, Japan*

I. Khmyrova, M. Ryzhii, and V. Ryzhii*

Computer Solid State Physics Laboratory, University of Aizu, Aizu-Wakamatsu 965-8580, Japan

M. S. Shur

*Department of Electrical, Computer and Systems Engineering,
Rensselaer Polytechnic Institute, Troy 12180, U.S.A*

(Dated: October 25, 2018)

We study plasma effects in a micromachined high-electron mobility transistor (HEMT) with the microcantilever serving as the gate using the developed a model. The model accounts for mechanical motion of the microcantilever and spatio-temporal variations (plasma effects) of the two-dimensional electron gas(2DEG) system in the transistor channel. The microcantilever mechanical motion is described in the point-mass approximation. The hydrodynamic electron transport model is used to describe distributed electron plasma phenomena in the 2DEG system. Using the developed model, we calculated the response function characterizing the amplitude microcantilever oscillations and the output electric signal as functions of the signal frequency and the bias voltage for the devices with different parameters. We find the voltage dependences of the frequency of the mechanical resonance and its damping. In particular, it is demonstrated that the amplitudes of the mechanical oscillations and output electric signal exhibit pronounced maxima at the bias voltages close to the voltage of the 2DEG channel depletion followed by a steep drop with further increase in the bias voltage.

PACS numbers: 73.50.Mx, 73.40.-c, 73.43.Cd

PACS numbers:

I. INTRODUCTION

The concept of a field-effect transistor with a micro-machined cantilever as floating gate was put forward and discussed a long time ago by Nathanson *et al* [1] (see, also ref. [2]). Recently [2], this concept was further evolved and a floating-gate high-electron-mobility transistor (HEMT) device comprising a microcantilever over a two-dimensional electron gas (2DEG) channel was fabricated and measured (see, for instance, also refs. [3, 4, 5, 6, 7]). A theoretical assessment of this and similar devices is usually based on equations governing the mechanical motion of the cantilever supplemented by some circuit equations. However, the motion of the electrically actuated microcantilever results in a complex motion of electrons in the 2DEG channel, which, in turn, leads to variations of the electron sheet density and the self-consistent electric field affecting the microcantilever dynamics. The simplest effect of 2DEG in micromachined HEMTs is associated with a finite conductivity of the latter, particularly at the voltages corresponding to a significant depletion of the 2DEG channel. The electron transient processes associated with the variations of the electron sheet density and the self-consistent electric field, i.e., electron plasma processes, can play a

significant role in HEMTs and different HEMT-based devices [8, 9, 10, 11, 12, 13] (see also experimental papers [14, 15, 16, 17, 18, 19, 20]). The plasma effects in the HEMT-like devices can result in resonant response at the frequencies coinciding with the frequencies of plasma oscillations. Since these frequencies usually fall into the terahertz range, such effects are important in different terahertz devices. Despite a substantial difference in the resonant mechanical frequencies and the characteristic plasma frequencies, micromachined elements such as a microcantilever floating-gate may be useful for terahertz devices. For instance, the microcantilever floating gate can be used for the internal modulation of terahertz signals in the resonant detectors utilizing the excitation of plasma oscillations (see, for example, ref. [8]). The consideration of plasma effects in the HEMT-like devices requires a device model which adequately describes spatio-temporal variations of the 2DEG system.

In this work, we develop a model which self-consistently describes the mechanical oscillations of a highly conducting (metallized) microcantilever and the dynamic properties of the 2DEG system. The model is based on an equation governing oscillations of a microcantilever under mechanical and electric forces and hydrodynamic equations governing the electron transport in 2DEG. Our model accounts for such phenomena as the depletion and enrichment of 2DEG by the applied voltage in the presence of the surface charges at the semiconductor surface beneath the microcantilever

*Electronic address: v-ryzhii@u-aizu.ac.jp

and finiteness of the 2DEG conductivity, the delay in the electron recharging under the microcantilever (gate) and the spatial nonuniformity of the potential distribution in the 2DEG, which might affect the device characteristics. Thus, the model under consideration is a distributed (physical) model which provides more general and detailed description of the underlying processes than that based on the treatment of the electron system of the device invoking electric circuit models. Generally, the device under consideration is similar to those fabricated and studied both theoretically and experimentally, in particular, in refs. [1, 2]. The main distinction is that in micromachined HEMTs investigated in refs. [1, 2] there are two metallized surfaces: one at the bottom of the microcantilever and one covering a portion of the semiconductor surface under the microcantilever (the so-called input force plate [1]). In contrast, we assume that the microcantilever motion is due to the interaction of the charge induced in the microcantilever metallized surface and the charge in the 2DEG channel. Thus, the 2DEG channel plays the dual role: it is used for the microcantilever actuation and the variation of its conductivity is used to detect the output signals. The effectiveness of the control of the 2DEG channel by applying voltage to the microcantilever was demonstrated experimentally even in ref. [1] (see, also ref. [2] and references therein). The effect of interaction of the charges induced in the microcantilever and the conducting plane electrode was theoretically considered recently in ref. [21]. However, the model used in ref. [21] assumes, in contrast to our model, that the electrode is ideally conducting that is not always the case in real 2DEG channels.

The developed model is used to study the resonant response of the device to the ac signals. We find the dependences of the resonance frequency and the resonance width on the both mechanical and electron properties of the system under consideration. In particular, we demonstrate that the plasma effects in the 2DEG channel can give rise to a shift of the resonance and an increase in the oscillation damping, i.e., limit the quality factor of the microcantilever oscillations. We show also that relatively high-frequency signals (with the frequency corresponding to the plasma resonance) can result in a significant variation of the microcantilever position.

The paper is organized as follows. In Sec. 2, we discuss the device model and write down the pertinent equations. Section 3 deals with a small-signal analysis based on the linearized versions of equations of the model. In this section, we calculate the spatial distributions of the ac potential and electron density in the 2DEG channel and find the amplitude (response function) of the microcantilever oscillations as a function of the signal frequency and the bias voltage. In Sec. 4, we analyze the response function in different limiting cases and demonstrate the results of numerical calculations of the device characteristics using the formulas obtained in the previous sections. Section 5 deals with the calculations of the output source-to-drain ac current and the effective device transconductance. In

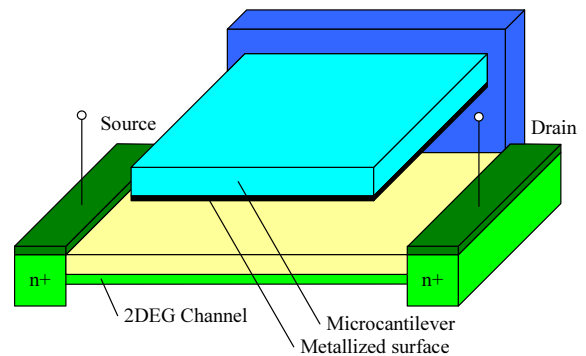


FIG. 1: Schematic view of device structure.

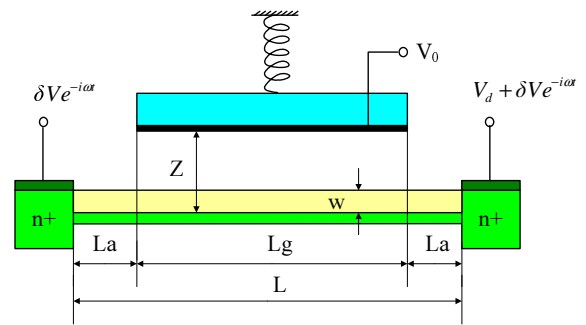


FIG. 2: Device model.

Sec. 6, we consider the effect of high-frequency signals (on the variation of the microcantilever position associated with the plasma resonance. In conclusion (Sec. 7), we draw the main results. Some ancillary calculations are factored out to Appendix A and Appendix B.

II. EQUATIONS OF THE MODEL

The device structure under consideration is schematically shown in Fig. 1. It is assumed that the voltage applied between the metallized cantilever, which serves as the HEMT floating gate, and the side contacts to 2DEG channel (HEMT's source and drain) comprises the dc (V_0) and ac (δV) components. Focusing on fairly detailed description of the electron transport in the 2DEG channel accompanying the microcantilever oscillations, we shall consider the cantilever mechanical properties in the framework of a simplified model, namely, using the so-called point-mass model [22] (see Fig.2). This model assumes that consideration of the elastic microcantilever or beam is replaced by the consideration of a point mass M (cantilever effective mass) attached to a string with stiffness K with M and K chosen such that the resonant frequency of the microcantilever oscillations associated solely with its mechanical properties, $\Omega_0 = \sqrt{K/M}$. In this model, the displacement of the cantilever (gate) is

governed by the following equation:

$$M \left[\frac{\partial^2 Z}{\partial t^2} + \gamma_0 \frac{\partial Z}{\partial t} + \Omega_0^2 (Z - W) \right] = eD \int_{-L_g/2}^{L_g/2} dx \mathcal{E} (\Sigma - \Sigma_d + \Sigma_s), \quad (1)$$

where $Z = Z(t)$ is the distance between the cantilever surface and the 2DEG, W is this distance in the absence of the applied voltage in equilibrium, γ_0 is the damping of the cantilever oscillations associated with different mechanisms of the energy loss in the cantilever body and in the clamp, $e = |e|$ is the value of the electron charge, D and L_g are the pertinent sizes of the cantilever (see, Fig.2), $\Sigma = \Sigma(t, x)$ is the electron sheet density of 2DEG, $\Sigma_d = \text{const}$ is the donor sheet density, and $\Sigma_s = q_s/e$, where q_s is the sheet density of the surface charge at the interface between the semiconductor and the gas (or vacuum), which does not change when the microcantilever moves. The surface charge corresponds to the surface potential $V_s = 4\pi e w \Sigma_s / \epsilon$. The electric field $\mathcal{E} = \mathcal{E}(t, x)$ at the microcantilever plane is determined by the potential drop $V_0 - V_s - \varphi$, where $\varphi = \varphi(t, x)$ is the potential of 2DEG. Here, the axis z is directed perpendicular to the 2DEG plane, while the axis x is directed in the 2DEG plane. Equation (1) is valid in the case of a highly conducting (metallized) cantilever when its surface is equipotential. The microcantilever and 2DEG are separated by two layers: the isolation solid layer of thickness w and dielectric constant ϵ and the layer of a gas (or vacuum) of thickness $Z - w$ and dielectric constant $\epsilon^* \simeq 1$ (see Figs. 1 and 2). The term in the right-hand side of eq. (1) represents the electric force acting on the microcantilever due the applied voltage.

In the gradual channel approximation valid if $Z, W \ll L_g$, [23]

$$\mathcal{E} = \frac{(\varphi - V_0 + V_s)}{[Z - w(1 - \epsilon^*/\epsilon)]} = -\frac{4\pi e}{\epsilon^*} (\Sigma - \Sigma_d + \Sigma_s). \quad (2)$$

Equations (1) and (2) disregard the effect of fringing capacitance, [23] which can appear at the bias voltages beyond the essential depletion of the gated portion of the 2DEG channel (this voltage range is not considered here).

Equations (1) and (2) lead to

$$\frac{\partial^2 Z}{\partial t^2} + \gamma_0 \frac{\partial Z}{\partial t} + \Omega_0^2 (Z - W) = -\frac{D}{4\pi M} \int_{-L_g/2}^{L_g/2} dx \mathcal{E}^2, \quad (3)$$

where $Z \geq w$ and $\Sigma \geq 0$. In the following, we put for simplicity $\epsilon^* = 1$.

Equations (2) and (3) should be supplemented by the hydrodynamic equations (continuity equation and Euler equation) governing the electron transport in 2DEG [8, 9]:

$$\frac{\partial \Sigma}{\partial t} + \frac{\partial \Sigma u}{\partial x} = 0, \quad (4)$$

$$\frac{\partial u}{\partial t} + u \frac{\partial u}{\partial x} + \nu u = \frac{e}{m} \frac{\partial \varphi}{\partial x}. \quad (5)$$

Here, $u = u(t, x)$ is the average (hydrodynamic) electron velocity in the 2DEG plane, ν is the electron collision frequency, and m is the electron effective mass. The electron collision frequency is expressed via the 2DEG mobility μ as $\nu = e/m\mu$.

III. SMALL-SIGNAL ANALYSIS

Let us assume that the net voltage between the cantilever (gate) and the side contacts to the 2DEG (source and drain) apart from dc components (V_0 and $V_0 + V_D$) comprises also the ac component $\delta V \exp(-i\omega t)$: where δV ($|\delta V| \ll V_0$) and ω are the amplitude and frequency of the ac voltage. The drain-to-source voltage V_D is assumed to be sufficiently small and corresponds to the linear region of the HEMT operation. Considering small oscillations of the cantilever and the electron density, one can assume

$$Z(t) = Z_0 + \delta Z \exp(-i\omega t),$$

$$\Sigma(t, x) = \Sigma_0 + \delta \Sigma \exp(-i\omega t),$$

$$u(t, x) = \delta u \exp(-i\omega t),$$

$$\varphi(t, x) = \delta \varphi \exp(-i\omega t),$$

where the amplitudes δZ , $\delta \Sigma$, δu , and $\delta \varphi$ are assumed to be small in comparison with the steady-state separation, Z_0 , between the microcantilever and the 2DEG channel (see Appendix A). Here $\Sigma_0 = \Sigma_d - \Sigma_s + [(V_0 - V_s)/4\pi e Z_0] \simeq \Sigma_d - \Sigma_s + (V_0/4\pi e Z_0)$ is the dc electron density in the gated portion of the 2DEG channel. In the above equation (and in the following), we have omitted for brevity the term with V_s because of its smallness (it is proportional to small values w and ϵ^{-1} : $V_s \propto w \Sigma_s / \epsilon$). Nevertheless, the direct contribution of the surface charges to the dc electron density is taken into account. Considering the smallness of the above-mentioned amplitudes of variations, eqs. (1) - (5) can be linearized. As a result, neglecting $w(1 - \epsilon^{-1})$ in comparison with Z_0 , we arrive at

$$(\Omega_0^2 - i\gamma\omega - \omega^2)\delta Z = \left(\frac{V_0^2}{2\pi Z_0^2} \frac{DL_g}{M} \right) \frac{\delta Z}{Z_0} + \left(\frac{V_0^2}{2\pi Z_0^2} \frac{DL_g}{M} \right) \frac{1}{L_g} \int_{-L_g/2}^{L_g/2} dx \frac{\delta \varphi}{V_0}, \quad (6)$$

$$\delta \Sigma = -\frac{1}{4\pi e Z_0} \left(\delta \varphi + V_0 \frac{\delta Z}{Z_0} \right), \quad (7)$$

$$-i\omega \delta \Sigma + \Sigma_0 \frac{d\delta u}{dx} = 0, \quad (8)$$

$$(\nu - i\omega)\delta u = \frac{e}{m} \frac{d\delta\varphi}{dx} \quad (9)$$

$$\frac{d^2\delta\varphi}{dx^2} + \frac{m\omega(\omega + i\nu)}{4\pi e^2 \Sigma_0 Z_0} \delta\varphi = -\frac{m\omega(\omega + i\nu)V_0}{4\pi e^2 \Sigma_0 Z_0} \frac{\delta Z}{Z_0} \quad (10)$$

or introducing the characteristic plasma velocity S as

$$S = \sqrt{\frac{4\pi e^2 \Sigma_0 Z_0}{m}}, \quad (11)$$

we obtain the following equations

$$\begin{aligned} & \left[\Omega_0^2 - \Omega_0^2 \left(\frac{V_0}{\bar{V}_0} \right)^2 - i\gamma_0\omega - \omega^2 \right] \delta Z \\ &= \Omega_0^2 \left(\frac{V_0}{\bar{V}_0} \right)^2 \frac{Z_0}{L_g} \int_{-L_g/2}^{L_g/2} dx \frac{\delta\varphi}{V_0}, \end{aligned} \quad (12)$$

and

$$\frac{d^2\delta\varphi}{dx^2} + \frac{\omega(\omega + i\nu)}{S^2} \delta\varphi = -\frac{\omega(\omega + i\nu)V_0}{S^2} \frac{\delta Z}{Z_0}. \quad (13)$$

The boundary conditions for eq. (13) can be chosen considering that the amplitude of the ac potential of the side contacts is equal to δV and taking into account the ac potential drop across the access sections of the channel (see Fig. 2), i.e., the regions between the gate edges and the side contacts. Assuming that the electron collision frequencies in different regions of the 2DEG channel are the same and neglecting the deviation of the electron sheet density in the access regions from the donor density Σ_d , the boundary conditions can be presented as [24]

$$\delta\varphi|_{x=\pm L_g/2} = \delta V - L_a \left(\frac{\Sigma_0}{\Sigma_d - \Sigma_s} \right) \frac{d\varphi}{dx} \Big|_{x=\pm L_g/2}. \quad (14)$$

Consider first the device structure in which the length, L_a , of the access (ungated) sections, is sufficiently small in comparison with the gate length L_g (i.e., $L_a \ll L_g \Sigma_d / \Sigma_0$). In this case, one can neglect the ac potential drop across the access regions of the 2DEG channel, i.e., the second term in the right-hand side of eq. (14) [11, 24]. As a result, from eqs. (13) and (14) we obtain

$$\begin{aligned} \delta\varphi = & \frac{V_0}{Z_0} \left[\frac{\cos \left[\frac{\sqrt{\omega(\omega + i\nu)} x / S}{\cos \left[\frac{\sqrt{\omega(\omega + i\nu)} L_g / 2S \right]} - 1 \right]}{\cos \left[\frac{\sqrt{\omega(\omega + i\nu)} L_g / 2S \right]} - 1 \right] \delta Z \\ & + \frac{\cos \left[\frac{\sqrt{\omega(\omega + i\nu)} x / S}{\cos \left[\frac{\sqrt{\omega(\omega + i\nu)} L_g / 2S \right]} \right]}{\cos \left[\frac{\sqrt{\omega(\omega + i\nu)} L_g / 2S \right]} \delta V. \end{aligned} \quad (15)$$

Substituting $\delta\varphi$ from eq. (15) to eq. (12), we arrive at

$$\frac{\delta Z}{\delta V} = \frac{Z_0}{V_0} \mathcal{Z}_\omega, \quad (16)$$

where

$$\mathcal{Z}_\omega = \frac{\Omega_0^2 (V_0 / \bar{V}_0)^2 (\tan Q_\omega / Q_\omega)}{[\Omega_0^2 - i\gamma_0\omega - \omega^2 - \Omega_0^2 (V_0 / \bar{V}_0)^2 (\tan Q_\omega / Q_\omega)]}. \quad (17)$$

Here, we have introduced

$$Q_\omega = \frac{\pi}{2} \frac{\sqrt{\omega(\omega + i\nu)}}{\Omega_p}, \quad \bar{V}_0 = \sqrt{\frac{2\pi\Omega_0^2 M W^3}{L_g D}}, \quad (18)$$

where

$$\Omega_p = \frac{\pi S}{L_g} = \sqrt{\frac{4\pi^3 e^2 \Sigma_0 Z_0}{m L_g^2}} = \Omega_{p0} \sqrt{\frac{\Sigma_0 Z_0}{(\Sigma_d - \Sigma_s) W}} \quad (19)$$

is the characteristic plasma frequency of the gated 2DEG channel and $\Omega_{p0} = \sqrt{4\pi^3 e^2 (\Sigma_d - \Sigma_s) W / m L_g^2}$

One can see that Ω_p depends on the bias voltage via the voltage dependence of Σ_0 and Z_0 . The Ω_p versus V_0 dependence is asymmetric; The plasma frequency can be significantly decreased by negative bias when the 2DEG channel becomes close to the depletion.

The finiteness of the conductivity of the access ungated regions can also contribute to the damping of the microcantilever oscillations. This can occur when the length of this regions L_a is sufficiently large. To include these regions into the model, we need to modify boundary condition (19) to take into account the potential drop across them. Generally, the access regions can pronouncedly affect the plasma phenomena in HEMTs [11, 14, 23], in particular, leading to a decrease in the characteristic plasma frequencies.

Preserving the second term in the right-hand side of eq. (4) associated with the contribution of the access region to the boundary conditions, we arrive at

$$\mathcal{Z}_\omega = \frac{\Omega_0^2 (V_0 / \bar{V}_0)^2 (\tan Q_\omega / Q_\omega^*)}{\{\Omega_0^2 - i\gamma_0\omega - \omega^2 - \Omega_0^2 (V_0 / \bar{V}_0)^2 (\tan Q_\omega / Q_\omega^*)\}}, \quad (20)$$

where $Q_\omega^* = Q_\omega (1 - \alpha \tan Q_\omega)$ and $\alpha = (2L_a / L_g) [\Sigma_0 / (\Sigma_d - \Sigma_s)]$ is the parameter characterizing the role of the access regions. At $\alpha = 0$, $Q_\omega^* = Q_\omega$ and eqs. (17) and (20) coincide.

IV. MICROCANTILEVER FORCED OSCILLATIONS (ANALYSIS OF LIMITING CASES AND NUMERICAL CALCULATIONS)

A. Highly conducting 2DEG channel

In many practical situations, the signal frequency ω is in the same range as the resonant frequency of the

microcantilever oscillations Ω_0 and the conductivity of the 2DEG channel is rather large. The latter corresponds to $\Omega_p \gtrsim \nu$. Since usually $\omega, \Omega_0 \ll \nu, \Omega_p$, the quantity $|Q_\omega| \ll 1$, and eqs. (17) and (20) can be simplified. In such a case, one obtains $\tan Q_\omega/Q_\omega \simeq 1 + Q_\omega^2/3 \simeq 1 + i(\pi^2/12)(\omega\nu/\Omega_p^2)$. Considering this, assuming that $\alpha \ll 1$ and using eq. (17), the response function \mathcal{Z}_ω can be presented in the standard form

$$\mathcal{Z}_\omega \simeq \frac{\Omega_0^2}{(\Omega_m^2 - i\gamma_m\omega - \omega^2)} \left(\frac{V_0}{\bar{V}_0}\right)^2. \quad (21)$$

Here, however, the resonant frequency Ω and the quantity characterizing the damping of oscillations γ depend on the ‘‘electron’’ parameters:

$$\begin{aligned} \Omega_m &= \Omega_0 \sqrt{1 - \left(\frac{V_0}{\bar{V}_0}\right)^2}, \quad (22) \\ \gamma_m &= \gamma_0 + \nu \left(\frac{\pi^2}{12}\right) \left(\frac{\Omega_0}{\Omega_p}\right)^2 \left(\frac{V_0}{\bar{V}_0}\right)^2 \\ &\simeq \gamma_0 + \nu \frac{\left(\frac{\pi^2}{12}\right) \left(\frac{\Omega_0}{\Omega_{p0}}\right)^2 \left(\frac{V_0}{\bar{V}_0}\right)^2}{\left[1 + \beta \left(\frac{V_0}{\bar{V}_0}\right) - \frac{1}{2} \left(\frac{V_0}{\bar{V}_0}\right)^2\right]}, \quad (23) \end{aligned}$$

where $\beta = \bar{V}_0/|V_0^{(depl)}|$ and $V_0^{(depl)}$ is the characteristic depletion voltage or HEMT’s threshold voltage. Here we have considered the dependence of the characteristic plasma frequency on Σ_0 and the dependence of the latter on the bias voltage (see Appendix B, eq. (B2)). As seen from eq. (21), the resonant frequency is equal to Ω . The modulus of the response function $|\mathcal{Z}_\omega|$ is given by

$$|\mathcal{Z}_\omega| = \frac{\Omega_0^2}{\sqrt{(\Omega_m^2 - \omega^2)^2 + \gamma_m^2\omega^2}} \left(\frac{V_0}{\bar{V}_0}\right)^2, \quad (24)$$

so that at the resonance

$$\max|\mathcal{Z}_\omega| = \frac{\Omega_0^2}{\gamma_m\Omega_m} \left(\frac{V_0}{\bar{V}_0}\right)^2. \quad (25)$$

The second term in the right-hand side of eq. (23) proportional to $\nu/\Omega_p^2 \propto \nu/\Sigma_0$ (i.e., proportional to the resistance of the gated region of the 2DEG channel) determines the contribution to the resonance width associated with the dissipation processes in the gated 2DEG channel due to the finiteness of its conductivity. Equation (24) demonstrates a tendency for γ_m to increase with approaching to the 2DEG channel depletion. If the second term in the right-hand side of eq. (23) becomes dominant, it might limit the quality factor of the microcantilever oscillations: $Q_m = \Omega_m/\gamma_m < Q_0 = \Omega_0/\gamma_0$. For example, for $\Omega_0/2\pi = 100$ MHz, $\Omega_p/2\pi = 50$ GHz, $\nu = 4 \times 10^{12} \text{ s}^{-1}$ (electron mobility $\mu = 8000 \text{ cm}^2/\text{Vs}$), and $V_0/\bar{V}_0 = 0.1$, that can correspond to a HEMT with GaAs channel close to depletion at room temperature, the quality factor is limited by the value $\max Q_m < 5 \times 10^3$.

B. Low conductivity of the 2DEG channel (low plasma frequency)

At a strong depletion of 2DEG channel at negative bias voltages, the conductivity of 2DEG channel and the plasma frequency can be relatively low. At low plasma frequency Ω_p when $\omega, \Omega_0 \gg \Omega_p^2/\nu$, one obtains $Q_\omega \simeq \pi\sqrt{i\omega\nu}/2\Omega_p$ with $|Q_\omega| = \pi\sqrt{\omega\nu}/2\Omega_p \gg 1$. In such a situation, $\tan Q_\omega/Q_\omega \simeq [(1+i)\sqrt{2}/\pi](\Omega_p/\sqrt{\nu\omega})$. Hence,

$$\mathcal{Z}_\omega \simeq \frac{\Omega_0^2(V_0/\bar{V}_0)^2[(1+i)\sqrt{2}\Omega_p/\pi\sqrt{\nu\omega}]}{\Omega_0^2 - i\gamma_\omega - \omega^2 - \Omega_0^2(V_0/\bar{V}_0)^2[(1+i)\sqrt{2}\Omega_p/\pi\sqrt{\nu\omega}]}. \quad (26)$$

As follows from eq. (26), when $\Omega_0 \gg \Omega_p^2/\nu$ at the resonance (compare with the pertinent formula for the case highly conducting 2DEG channel),

$$\max|\mathcal{Z}_\omega| \simeq \frac{\Omega_0}{\gamma_0} \left(\frac{2}{\pi} \frac{\Omega_p}{\sqrt{\nu\Omega_0}}\right) \left(\frac{V_0}{\bar{V}_0}\right)^2 \ll \frac{\Omega_0}{\gamma_0} \left(\frac{V_0}{\bar{V}_0}\right)^2. \quad (27)$$

Thus, in the case under consideration here, even at the resonance, $\max|\mathcal{Z}_\omega| \lesssim 1$. If $\sqrt{\nu/\Sigma_0}$, increases, i.e., the 2DEG channel conductivity decreases, $\max|\mathcal{Z}_\omega|$ markedly decreases as well. Hence, when the bias voltage V_0 approaches to the depletion voltage $V_0^{(depl)}$, the resonant peak markedly diminishes.

C. Mechanical response at plasma resonance

If the signal and plasma frequencies markedly exceed the electron collision frequency and the resonant frequency of pure mechanical oscillations of the microcantilever ($\omega, \Omega_p \gg \nu, \Omega_0$) and the signal frequency is close to one of the plasma frequencies $\Omega_p(2n-1)$, where $n = 1, 2, 3, \dots$ is the index of the plasma mode, the quantity $|\tan Q_\omega/Q_\omega|$ can be rather large. At the fundamental plasma resonance $\tan Q_\omega/Q_\omega \simeq i(4/\pi^2)(\Omega_p/\nu)$. Taking this into account, from Eq. (18) we find that as in the case considered in the previous subsection, $\max|\mathcal{Z}_\omega| \lesssim 1$. One can also find that when Ω_p/ν increases to infinity, $\max|\mathcal{Z}_\omega|$ formally tends to unity. However, in most realistic cases ($\Omega_0 \lesssim \nu \ll \Omega_p$ and $V_0 < \bar{V}_0$),

$$\max|\mathcal{Z}_\omega| \simeq \frac{4}{\pi^2} \left(\frac{\Omega_0^2}{\nu\Omega_p}\right) \left(\frac{V_0}{\bar{V}_0}\right)^2 \ll 1. \quad (28)$$

This shows that even at rather sharp plasma resonance, the amplitude of the microcantilever oscillations remains small in comparison with the amplitude at the mechanical resonance at $\omega = \Omega$. Indeed, the ratio of $\max|\mathcal{Z}_\omega|$ at $\omega = \Omega_p$ and at $\omega = \Omega$ can be estimated as

$$\frac{\max|\mathcal{Z}_\omega|_{\omega=\Omega_p}}{\max|\mathcal{Z}_\omega|_{\omega=\Omega}} \simeq \frac{\pi^2}{4} \frac{\gamma_0\Omega_0}{\nu\Omega_p} \ll 1. \quad (29)$$

At the plasma resonance, the amplitude of the ac electric field in the gated region can be rather large.

D. Role of the access regions

Consider now the case when α is not small invoking Eq. (20). When $\omega, \Omega_0 \ll \nu, \Omega_p$, one obtains $|Q_\omega| = \pi\sqrt{\omega\nu}/2\Omega_p \ll 1$ and eq. (20) can be simplified. In the vicinity of the resonance $\omega \simeq \Omega_m$, where in the case under consideration (compare with eq. (22))

$$\Omega_m = \Omega_0 \sqrt{1 - \frac{(V_0/\bar{V}_0)^2}{[1 + \alpha^2(\pi/2)^4(\Omega_0\nu)^2/\Omega_p^4]}}, \quad (30)$$

one obtains

$$\mathcal{Z}_\omega \simeq \frac{\Omega_0^2(V_0/\bar{V}_0)^2}{(\Omega^2 - i\gamma\omega - \omega^2)[1 - i\alpha(\pi^2/4)(\omega\nu)/\Omega_p^2]}. \quad (31)$$

Here

$$\begin{aligned} \gamma_m &= \gamma_0 + \nu \left[\frac{\pi^2(1+3\alpha)}{12} \right] \frac{(\Omega_0/\Omega_p)^2}{[1 + \alpha^2(\pi/2)^4(\Omega_0\nu)^2/\Omega_p^4]} \left(\frac{V_0}{\bar{V}_0} \right)^2 \\ &= \gamma_0 + \nu \left[\frac{\pi^2(1+3\alpha)}{12} \right] \frac{(\Omega_0/\Omega_p)^2}{(1 + \Omega_0^2\tau_a^2)} \left(\frac{V_0}{\bar{V}_0} \right)^2 \end{aligned} \quad (32)$$

is the quantity characterizing the damping of oscillations. Here $\tau_a = \alpha(\pi^2/4)\nu/\Omega_p^2$ is the RC-delay time: $\tau_a = R_a C_g$, where $R_a = (m\nu L_a/2e^2\Sigma_d)$ and $C_g = L_g/4\pi Z_0$ are the resistance of the access regions and the effective capacitance of the gated portion of the 2DEG channel, respectively. When $\alpha(\pi^2/4)(\Omega_0\nu)/\Omega_p^2 = \Omega_0\tau_a \sim 1$, eq. (32) results in

$$\gamma_m \simeq \gamma_0 + \nu \left(\frac{\pi^2\alpha}{8} \right) \left(\frac{\Omega_0}{\Omega_p} \right)^2 \left(\frac{V_0}{\bar{V}_0} \right)^2 \quad (33)$$

One can see that the second term in the right-hand side of eq. (33) differs from the pertinent term in eq. (23) by a factor $3\alpha/2$ which can be large (when $L_a \gg L_g$).

Equation (31) leads to

$$|\mathcal{Z}_\omega| \simeq \frac{\Omega_0^2}{\sqrt{(\Omega_m^2 - \omega^2)^2 + \gamma_m^2\omega^2}} \sqrt{1 + \omega^2\tau_a^2} \left(\frac{V_0}{\bar{V}_0} \right)^2. \quad (34)$$

At the exact mechanical resonance $\omega = \Omega_m$, from eq. (34), we obtain

$$\max|\mathcal{Z}_\omega| \simeq \frac{\Omega_0}{\gamma_m \sqrt{1 + \Omega_m^2\tau_a^2}} \left(\frac{V_0}{\bar{V}_0} \right)^2. \quad (35)$$

One needs to point out that the second terms in the right-hand side of eqs. (24) and (34) are the products of small factors, $(\Omega_0/\Omega_p)^2$ and $(V_0/\bar{V}_0)^2$, and relatively large value ν (normally $\nu \gg \gamma_0$).

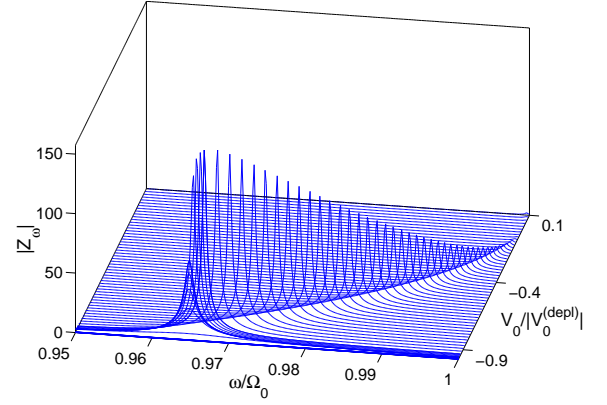


FIG. 3: Modulus of the response function $|\mathcal{Z}_\omega|$ as a function of normalized signal frequency ω/Ω_0 at different bias voltages $\beta V_0/\bar{V}_0 = V_0/|V_0^{(depl)}|$.

E. Results of numerical calculations

Figure 3 shows the modulus of the response function $|\mathcal{Z}_\omega|$ determined by Eq. (20) versus signal frequency calculated for AlGaAs/GaAs micromachined HEMT devices under consideration at different bias voltages. The device parameters are chosen as follows: $\Omega_0/2\pi = 100$ MHz, $Q_0 = \Omega_0/\gamma_0 = 2500$, $\Omega_{p0}/2\pi = 1$ THz, and $\nu = 10^{12}$ s $^{-1}$. The above parameters correspond to a AlGaAs/GaAs HEMT-based device with to $L_g = 2$ μm , $L_a = 1$ μm , $W = 0.5$ μm , $M/L_gD = 4 \times 10^{-12}$ g/ μm^2 , $\Sigma_d - \Sigma_s = 1 \times 10^{11}$ cm $^{-2}$, and the electron mobility $\mu = 3 \times 10^4$ cm 2 /Vs. At the above parameters, $\Omega_{p0}/\Omega_0 = 10^4$, $\nu/\Omega_0 = 10^4/2\pi$, $\bar{V}_0 = 33$ V, $V_0^{(depl)} = -9$ V (so that $\beta = 3.67$), and $V_0^{(pull-in)} = 18$ V. It is seen from Fig. 3 that the resonant frequency decreases with increasing bias voltage (in line with eq. (22)). Figure 3 also shows that $|\mathcal{Z}_\omega|$ increases with increasing V_0 reaching a maximum at the voltage slightly smaller than the depletion voltage V_0^{depl} . Further increase in V_0 leads to a drastic drop in $|\mathcal{Z}_\omega|$. This is confirmed by Fig. 4 which shows the voltage dependence of max $|\mathcal{Z}_\omega|$ calculated for the above parameters (curve 1). The results of calculations for a device with $\Sigma_d - \Sigma_s = 3 \times 10^{11}$ cm $^{-2}$ and $L_g = 2$ μm are shown in Fig. 4 as well. The parameters related to curve 1 in Fig. 4 correspond to $|V_0^{(depl)}| < V_0^{(pull-in)}$, in contrast to curve 2 for which $|V_0^{(depl)}| > V_0^{(pull-in)}$.

V. OUTPUT ELECTRIC SIGNAL

The ac voltage applied between the microcantilever and the source and drain contacts and the microcantilever oscillations both result in the modulation of the electron density in the 2DEG channel and, therefore, in the modulation of the source-to-drain current. Indeed, using eqs. (7) and (15), one can obtain (for the case of

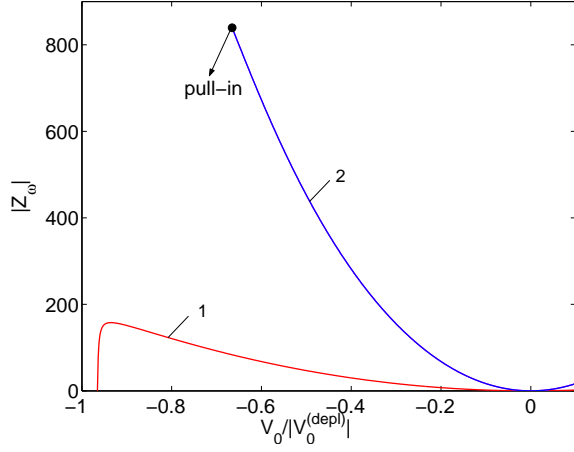


FIG. 4: Maximum (resonant) value of $|Z_\omega|$ as a function of normalized bias voltage $\beta V_0/\bar{V}_0 = V_0/|V_0^{(depl)}|$ calculated for different structural parameters: 1 - $\Sigma_d - \Sigma_s = 1 \times 10^{11} \text{ cm}^{-2}$ and 2 - $\Sigma_d - \Sigma_s = 3 \times 10^{11} \text{ cm}^{-2}$.

short access regions and relatively small signal frequencies)

$$\begin{aligned} \delta\Sigma &\simeq -\frac{(1+Z_\omega)}{4\pi e Z_0} \frac{\cos[\sqrt{\omega(\omega+i\nu)}x/S]}{\cos[\sqrt{\omega(\omega+i\nu)}L_g/2S]} \delta V \\ &\simeq -\frac{(1+Z_\omega)}{4\pi e Z_0} \frac{\cos[\sqrt{i\omega\nu}x/S]}{\cos[\sqrt{i\omega\nu}L_g/2S]} \delta V \simeq -\frac{(1+Z_\omega)}{4\pi e Z_0} \delta V. \end{aligned} \quad (36)$$

At the signal frequencies close to the microcantilever resonant frequency, i.e., at the frequencies significantly lower than the HEMT characteristic frequencies, one can use the transistor steady-state characteristics. As a result, the ac component of the drain current, which can be considered as the output signal, at low drain-to-source voltages $V_d \ll |V_0|$ is given by

$$\delta J_d = \frac{e\mu V_d}{L_g} \delta\Sigma. \quad (37)$$

Using eqs. (36) and (37), one obtains

$$\delta J_d = -\frac{g_0 V_d}{4\pi e \Sigma_d Z_0} (1+Z_\omega) \delta V \simeq \frac{g_0 V_d}{V^{(depl)}} (1+Z_\omega) \delta V, \quad (38)$$

where $g_0 = e\mu\Sigma_d/L_g$ is the conductance of the undepleted 2DEG channel. Accounting for eq. (17), from eq. (38) we obtain the following formula for the effective transconductance $g_m = -(\partial J_d/\partial V)|_{V_d=const}$ of the micromachined HEMT under consideration:

$$\begin{aligned} \frac{g_m}{g_0} &= \frac{V_d}{V^{(depl)}} (1+Z_\omega) \\ &= \frac{V_d}{|V^{(depl)}|} \left[1 + \frac{\Omega_0^2 (V_0/\bar{V}_0)^2 (\tan Q_\omega/Q_\omega)}{[\Omega_0^2 - i\gamma_0\omega - \omega^2 - \Omega_0^2 (V_0/\bar{V}_0)^2 (\tan Q_\omega/Q_\omega)]} \right]. \end{aligned} \quad (39)$$

The effective transconductance g_m includes both the usual component associated with the direct electron density modulation by the ac voltage and the component associated with the microcantilever oscillations (proportional to Z_ω). In the limit of highly conducting 2DEG channel, eq. (39) can be presented as

$$\frac{g_m}{g_0} \simeq \frac{V_d}{|V^{(depl)}|} \left[1 + \frac{\Omega_0^2}{(\Omega^2 - i\gamma\omega - \omega^2)} \left(\frac{V_0}{\bar{V}_0} \right)^2 \right]. \quad (40)$$

As seen from eq. (40), at the resonant frequency, the modulus of the transconductance exhibits a rather high maximum:

$$\max \frac{|g_m|}{g_0} \simeq \frac{V_D}{|V^{(depl)}|} \frac{\Omega_0^2}{\gamma\Omega} \left(\frac{V_0}{\bar{V}_0} \right)^2 \simeq \frac{V_D}{|V^{(depl)}|} \frac{\Omega_0}{\gamma_0} \left(\frac{V_0}{\bar{V}_0} \right)^2. \quad (41)$$

Since in the devices with high quality factor of mechanical resonance $|Z_\omega|$ at the resonant frequency can be much larger than unity, the output signal in the micromachined HEMT can significantly exceed the output signal in HEMTs with solely electrical modulation. However, as the bias voltage is approached to the depletion voltage, the contribution of the microcantilever oscillations to the transconductance vanishes and the latter steeply drops to zero. As follows from eq. (41) and Figs. 3 and 4, the mechanical resonance provides very sharp peaks of $|Z_\omega|$ and, hence, the transconductance modulus.

VI. ELECTRIC-FIELD OSCILLATIONS NEAR THE PLASMA RESONANCE

Using eqs. (2) and (15), one can find the ac electric field $\delta\mathcal{E}$ as a function of δV and the signal frequency ω . As shown the previous section, in the range of signal frequencies where the ac electric field can exhibit the plasma resonances ($\omega \simeq \Omega_p \gg \Omega_0, \nu$), the ac displacement of the microcantilever is relatively small. Hence, one can neglect the first term in the right-hand side of eq. (16) and, as follows from eq. (2), put $\delta\mathcal{E} \simeq \delta\varphi/Z_1$. Here, $Z_1 = \langle Z \rangle$ is the dc position of the microcantilever under the dc electric field between the microcantilever and 2DEG channel and the average effect of the ac electric field (compare with eq. (A2)):

$$Z_1 = W - \frac{DL_g}{4\pi\Omega^2 M} \left[V_0^2 + \frac{1}{L_g} \int_{-L_g/2}^{L_g/2} dx \langle \mathcal{E}^2 \rangle \right], \quad (42)$$

where the symbol $\langle \dots \rangle$ means averaging over fast oscillations with the frequency $\omega \gg \Omega_0$. As a result, we arrive at the following equation:

$$\delta\mathcal{E} \simeq \frac{\cos[\sqrt{\omega(\omega+i\nu)}x/S]}{\cos[\sqrt{\omega(\omega+i\nu)}L_g/2S]} \frac{\delta V}{Z_1}. \quad (43)$$

Substituting $\delta\mathcal{E}$ from eq. (43) into eq. (42), averaging over high-frequency oscillations, we obtain

$$Z_1 \simeq Z_0 - W\mathcal{F}_\omega \left(\frac{\delta V}{\bar{V}_0} \right)^2 \left(\frac{W}{Z_1} \right)^2. \quad (44)$$

Here

$$\mathcal{F}_\omega = \frac{1}{4L_g} \int_{-L_g/2}^{L_g/2} dx \left| \frac{\cos[\sqrt{\omega(\omega + i\nu)} x/S]}{\cos[\sqrt{\omega(\omega + i\nu)} L_g/2S]} \right|^2 \quad (45)$$

At relatively low dc and ac voltages when $(W - Z_0)/W \ll 1$ and $(W - Z_1)/W \ll 1$ (see eq. (A4)), we obtain the following formula:

$$\frac{Z_1}{W} \simeq 1 - \frac{1}{2} \left(\frac{V_0}{\overline{V_0}} \right)^2 - \mathcal{F}_\omega \left(\frac{\delta V}{\overline{V_0}} \right)^2. \quad (46)$$

The second and third terms in the right-hand side of eq. (46) are associated with the microcantilever displacement due to the bias voltage and the ac signal, respectively. Assuming $\Omega_p \gg \nu$, we obtain

$$\mathcal{F}_\omega \simeq \frac{[1 + (2\Omega_p/\pi\omega) \sin(\pi\omega/2\Omega_p) \cos(\pi\omega/2\Omega_p)]}{8[\cos^2(\pi\omega/2\Omega_p) + (\pi\nu/4\Omega_p)^2]}. \quad (47)$$

As follows from eq. (47), the electric response function \mathcal{F} exhibits sharp resonances at $\omega = \Omega_p(2n - 1)$, where $n = 1, 2, 3, \dots$ is the resonance index, if $\Omega_p \gg \nu$. In the vicinity of the fundamental resonant frequency, i.e., at $\omega \simeq \Omega_p$, eq. (41) yields

$$\mathcal{F}_\omega \simeq \frac{1}{2\pi^2} \frac{\Omega_p^2}{[(\omega - \Omega_p)^2 + \nu^2/4]}. \quad (48)$$

At this resonance, one obtains

$$\max \mathcal{F}_\omega \simeq \frac{2}{\pi^2} \left(\frac{\Omega_p}{\nu} \right)^2 \gg 1. \quad (49)$$

Equation (49) implies that the position of the microcantilever can be very sensitive to the incoming ac signals if their frequency is close to one of the plasma resonant frequencies and the quality factor of the plasma oscillations $Q_p \propto \Omega_p/\nu \gg 1$. Hence the micromachined HEMT under consideration can serve as a mechanical resonant detector of microwave and terahertz radiation.

One may expect that at sufficiently strong ac signals, the microcantilever can be pulled-in to the surface of the isolating layer. Assuming, for simplicity that $V_0 = 0$, we obtain the following condition of the microcantilever pull-in under the effect of the ac voltage:

$$\left(\frac{\delta V}{\overline{V_0}} \right)^2 \geq \frac{8}{27\mathcal{F}_\omega}. \quad (50)$$

Using the estimate for $\max \mathcal{F}_\omega$, we obtain

$$\min \left(\frac{\delta V}{\overline{V_0}} \right)^2 \geq \frac{4\pi^2}{27} \left(\frac{\nu}{\Omega_p} \right)^2 \propto \frac{1}{Q_p^2}, \quad (51)$$

so that the minimum ac pull-in voltage can be estimated as

$$\min \delta V^{(pull-in)} \simeq \left(\frac{\nu}{\Omega_p} \right) \overline{V_0}. \quad (52)$$

Equation (54) shows that when the quality factor of the plasma oscillations is large, the microcantilever pull-in might occur at fairly modest ac signals. However, one may assume that the real situation is more complex because the transition of the microcantilever to the position corresponding to its pull-in to the isolating layer should be accompanied by the channel depletion and significant change in the resonant plasma frequency. Due to this, the dynamic of the microcantilever pull-in out of the scope of this paper.

VII. CONCLUSIONS

We developed a model for a micromachined HEMT with the microcantilever serving as the gate. The model is based on an equation of mechanical motion of the microcantilever in the point-mass approximation accompanied by hydrodynamic equations describing distributed electron plasma phenomena in the 2DEG channel. Using this model, we calculated the response function describing the amplitude microcantilever oscillations and the output electric signal as functions of the signal frequency and the bias voltage for the devices with different parameters. We found the voltage dependences of the frequency of the mechanical resonance and its damping. It was demonstrated that the amplitudes of the mechanical oscillations and output electric signal exhibit pronounced maxima at the voltages close to the voltage of the 2DEG channel depletion. However, further increase in the bias voltage results in a drastic drop of the mechanical and electrical response. We showed also that at the frequency corresponding to the plasma resonance the ac electric field between the microcantilever and the 2DEG channel can be rather strong. This can result in a significant variation of the microcantilever position by incoming high-frequency (terahertz) signals.

This work was partially supported by the Grant-in-Aid for Scientific Research (S) from the Japan Society for Promotion of Science, Japan. The work at RPI was partially supported by the Office of Naval Research, USA.

Appendix A. Stationary states and pull-in and depletion voltages

When the voltage applied between the gate and side contacts is constant, eqs. (2) - (5) yield $u = u_0 = 0$, $\varphi = \varphi_0 = 0$, and

$$\Sigma_0 = \Sigma_d - \Sigma_s + \frac{V_0 - V_s}{4\pi e[Z_0 - w(1 - \alpha^{-1})]} \quad (A1)$$

with Z_0 governed by the following equation:

$$Z_0 = W - \frac{L_g D}{4\pi \Omega_0^2 M} \frac{V_0^2}{[Z_0 - w(1 - \alpha^{-1})]^2}. \quad (A2)$$

Introducing

$$\bar{V}_0 = \sqrt{2\pi\Omega_0^2 MW(W^2/L_g D)},$$

eq. (2) can be presented in the following form:

$$\frac{Z_0}{W} = 1 - \frac{1}{2} \left(\frac{V_0}{\bar{V}_0} \right)^2 \left[\frac{W}{Z_0 - w(1 - \alpha^{-1})} \right]^2, \quad (\text{A3})$$

The states with Z_0 satisfying eqs. (A2) and (A3) exist if $|V_0| \leq V_0^{(pull-in)}$, where

$$V_0^{(pull-in)} = \sqrt{\frac{8}{27} \left[1 - \frac{w}{W} \left(1 - \frac{1}{\alpha} \right) \right]^3 \bar{V}_0} \\ \simeq \sqrt{\frac{8}{27}} \bar{V}_0 \quad (\text{A4})$$

is the so-called pull-in voltage [1]. One can find that when $|V_0| > V_0^{(pull-in)}$, eq. (A3), does not have roots. In this case, the only existing (and stable) stationary state corresponds to the attachment of the microcantilever to the isolation solid layer, i.e., to $Z_0 = w$. At $|V_0| = V_0^{(pull-in)}$, the microcantilever position is $Z_0 = Z_0^{(pull-in)}$, where

$$\frac{Z_0^{(pull-in)}}{W} = \frac{2}{3} + \frac{1}{3} \frac{w}{W} \left(1 - \frac{1}{\alpha} \right) \simeq \frac{2}{3}. \quad (\text{A5})$$

When $|V_0| < V_0^{(pull-in)}$, eq. (A3) has two solutions: one with $Z_0 < Z_0^{(pull-in)}$ (unstable) and one with $Z_0^{(pull-in)} < Z_0 < W$ (stable). At $|V_0| \ll V_0^{(pull-in)}$, the position of the microcantilever in the stable state is given by

$$\frac{Z_0}{W} \simeq 1 - \frac{1}{2} \left(\frac{V_0}{\bar{V}_0} \right)^2. \quad (\text{A6})$$

There exists the stable state (not governed by eq. (A3)) with $Z_0 = w$ as well.

As follows from eqs. (A2) - (A3), Z_0 decreases with increasing $|V_0|$ disregarding the sign of the gate voltage V_0 . However, at $V_0 < 0$, the 2DEG channel can be fully depleted, so that $\Sigma_0 = 0$. The depletion voltage (or HEMT's threshold voltage) $V_0^{(depl)}$ corresponding to $\Sigma_0 = 0$, as can be found from eqs. (A1) and (A3), is given approximately by

$$V_0^{(depl)} \simeq -4\pi e \Sigma_d W. \quad (\text{A7})$$

This voltage corresponds to

$$\frac{Z_0^{(depl)}}{W} = 1 - \frac{1}{2} \left(\frac{V_0^{(depl)}}{\bar{V}_0} \right)^2. \quad (\text{A8})$$

The second terms in the right-hand side of Eq. (A8) is rather small. Indeed, if $\Sigma_d = (1 - 10) \times 10^{11} \text{ cm}^{-2}$,

$L_g D = 25 \text{ } \mu\text{m}^2$, $W = 0.5 \text{ } \mu\text{m}$, $M = 10^{-10} \text{ g}$, and $\Omega_0/2\pi = 1 - 10 \text{ MHz}$, we obtain $\bar{V}_0 \simeq 33 - 330 \text{ V}$, $V_0^{(depl)} \simeq 9 - 90 \text{ V}$, and $V_0^{(pull-in)} \simeq 18 - 180 \text{ V}$. Since \bar{V}_0 and, hence, $V_0^{(pull-in)}$ strongly decrease with decreasing W , their values can be markedly smaller than those obtained in the above estimates. The ratio of $|V_0^{(depl)}|$ to $V_0^{(pull-in)}$ can be presented as

$$\frac{|V_0^{(depl)}|}{V_0^{(pull-in)}} \simeq \sqrt{\frac{27\pi e^2 \Sigma_d^2 L_g D}{\Omega_0^2 MW}} \quad (\text{A9})$$

When $V_0 < 0$ and $|V_0| > V_0^{(depl)}$, the charge densities in the microcantilever and channel do not change with varying V_0 ; they are equal to Σ_d . In this case, eq. (A3) should be replaced by

$$\frac{Z_0}{W} = 1 - \frac{1}{2} \left(\frac{V_0^{(depl)} V_0}{\bar{V}_0^2} \right) \left[\frac{W}{Z_0 - w(1 - \alpha^{-1})} \right]. \quad (\text{A10})$$

As a result, for the pull-in voltage under the condition of the channel depletion we obtain

$$V_0^{(pull-in)} = \frac{1}{2} \frac{\bar{V}_0^2}{V_0^{(depl)}} \left[1 - \frac{w}{W} \left(1 - \frac{1}{\alpha} \right) \right]^2 \simeq \frac{1}{2} \frac{\bar{V}_0^2}{V_0^{(depl)}} \quad (\text{A11})$$

and (compare with eq. (A5))

$$\frac{Z_0^{(pull-in)}}{W} = \frac{1}{2} \left[1 + \frac{w}{W} \left(1 - \frac{1}{\alpha} \right) \right] \simeq \frac{1}{2}. \quad (\text{A12})$$

Appendix B. Voltage and mechanical control of the plasma resonances

The expression for the characteristic plasma frequency Ω_p of the gated 2DEG channel given by eq. (20) is somewhat different from that obtained previously for the standard HEMTs. This frequency in micromachined HEMTs exhibits different voltage dependence. As follows from eq. (20), the resonant plasma frequency Ω_p depends not only on the electron density in the 2DEG channel but also on the spacing, Z_0 , between the microcantilever (gate) and 2DEG. This opens up the possibility of a mechanical control of the plasma frequency and, hence, different characteristics of the pertinent terahertz devices.

One can obtain the following dependence of the characteristic plasma frequency on the microcantilever displacement and the bias voltage.

$$\Omega_p = \Omega_{p0} \sqrt{\frac{\Sigma_0 Z_0}{\Sigma_d W}} \simeq \Omega_{p0} \sqrt{\left(1 + \frac{V_0}{|V_0^{(depl)}|} \right) \frac{Z_0}{W}}. \quad (\text{B1})$$

If V_0 is fixed, the dependence of the characteristic plasma frequency on the microcantilever displacement is given by

eq. (41): $\Omega_p \propto \sqrt{Z_0}$. Taking into account that the microcantilever displacement depends on the bias voltage (see eq. (A6) from Appendix A), we find the following voltage dependence of the characteristic plasma frequency:

$$\Omega_p \simeq \Omega_{p0} \sqrt{1 + \beta \left(\frac{V_0}{V_0} \right) - \frac{1}{2} \left(\frac{V_0}{V_0} \right)^2}, \quad (\text{B2})$$

where $\beta = \overline{V_0}/|V_0^{(depl)}|$. It differs from the pertinent formula for the standard HEMTs by the third term under the square root in the right-hand side of eq. (B2).

-
- [1] H. C. Nathanson, W. E. Newell, R. A. Wickstrom, and J. R. Davis, Jr., IEEE Trans. Electron Devices, **14**, 117 (1967).
- [2] W. H. Teh, R. Crook, C. G. Smith, H. E. Beere, and D. A. Ritchie, J. Appl. Phys. **97**, 114507 (2005).
- [3] R. G. Beck, M. A. Eriksson, R. A. Westervelt, K. L. Campman, and A. C. Gossard, Appl. Phys. Lett. **68**, 3763 (1996).
- [4] M. P. Schwarz, D. Grundler, I. Meinel, Ch. Heyn, and D. Heitmann, Appl. Phys. Lett. **76**, 3464 (2000).
- [5] H. Yamaguchi, S. Miyashita, and Y. Hirayama, Appl. Phys. Lett. **82**, 394 (2003).
- [6] K. L. Ekunchi and M. L. Roukes, Rev. Sci. Instr. **76**, 161101 (2005).
- [7] Y. Tsuchiya, K. Takai, N. Momo, T. Nagami, H. Mizuta, S. Oda, S. Yamaguchi, and T. Shimada, J. Appl. Phys. **100**, 094306 (2006).
- [8] M. Dyakonov and M. Shur, IEEE Trans. Electron Devices **43**, 1640 (1996).
- [9] M. S. Shur and V. Ryzhii, Int. J. High Speed Electron. Syst. **13**, 575 (2003).
- [10] V. Ryzhii, I. Khmyrova, and M. S. Shur, J. Appl. Phys. **91**, 1875 (2002).
- [11] A. Satou, V. Ryzhii, I. Khmyrova, M. Ryzhii, and M. S. Shur, J. Appl. Phys. **95**, 2084 (2004).
- [12] V. Ryzhii, A. Satou, I. Khmyrova, A. Chaplik, and M. S. Shur, J. Appl. Phys. **96**, 7625 (2004).
- [13] A. Satou, V. Ryzhii, and A. Chaplik, J. Appl. Phys. **98**, 034502 (2005).
- [14] V. Ryzhii, A. Satou, W. Knap, and M. S. Shur, J. Appl. Phys. **99**, 084507 (2006).
- [15] Y. Deng, R. Kersting, J. Xu, R. Ascazubi, X.-C. Zhang, M. S. Shur, R. Gaska, G. S. Simin, M. Asif Khan, and V. Ryzhii, Appl. Phys. Lett. **84**, 70 (2004).
- [16] W. Knap, J. Lusakowski, T. Parently, S. Bollaert, A. Cappy, V. V. Popov, and M. S. Shur, Appl. Phys. Lett. **84**, 2331 (2004).
- [17] J. Lusakowski, W. Knap, N. Dyakonova, L. Varani, J. Mateos, T. Gonzales, Y. Roelens, S. Bullaert, A. Cappy, and K. Karpierz, J. Appl. Phys. **97**, 064307 (2005).
- [18] F. Teppe, D. Veksler, V. Yu. Kacharovskii, A. P. Dmitriev, S. Rumyantsev, W. Knap, and M. S. Shur, Appl. Phys. Lett. **96**, 022102 (2005).
- [19] T. Otsuji, M. Hanabe and O. Ogawara, Appl. Phys. Lett. **85**, 2119 (2004).
- [20] M. Hanabe, T. Otsuji, T. Ishibashi, T. Uno, and V. Ryzhii, Jpn. J. Appl. Phys. **44**, 3842 (2005).
- [21] R. C. Batra, M. Porfiri and D. Spinello, J. Microelectromechanical Syst. **15**, 1175 (2006).
- [22] U. Rabe, K. Janser, and W. Arnold, Sci. Instrum. **67**, 3281 (1996).
- [23] M. Shur, *Physics of Semiconductor Devices*, Prentice Hall, New Jersey, 1990.
- [24] A. Sato, I. Khmyrova, V. Ryzhii, and M. S. Shur, Semicond. Sci. Technol. **18**, 460 (2003).